ARTICLES
https://doi.org/10.1038/s41566-021-00764-4

nature photonics

Experimental demonstration of memory-enhanced scaling for entanglement connection of quantum repeater segments

Yun-Fei Pu[1,2,4], Sheng Zhang[1,4], Yu-Kai Wu[1], Nan Jiang[1,3], Wei Chang[1], Chang Li[1] and Lu-Ming Duan[1]✉

The quantum repeater protocol is a promising approach for implementing long-distance quantum communication and large-scale quantum networks. A key idea of the quantum repeater protocol is to use long-lived quantum memories to achieve an efficient entanglement connection between different repeater segments, with polynomial scaling. Here, we report an experiment that realizes the efficient connection of two quantum repeater segments via on-demand entanglement swapping through the use of two atomic quantum memories with storage times of tens of milliseconds. With the memory enhancement, acceleration in the scaling is demonstrated in the rate for a successful entanglement connection. Experimental realization of the entanglement connection of two quantum repeater segments with an efficient memory-enhanced scaling demonstrates a key advantage of the quantum repeater protocol, creating a cornerstone for the development of future large-scale quantum networks.

Long-distance quantum communication and large-scale quantum networks are central goals in quantum information science[1]. Direct communication of quantum signals in optical fibres is hindered by the inevitable exponential loss of photons with communication distance. The quantum repeater protocol provides a promising approach to solve this problem[2–4], with long-distance communication established through entanglement connection of many smaller segments of the communication channels, and with the exponential growth of noise being suppressed through heralding and nested entanglement purification[2,5,6]. A well-known approach to the implementation of quantum repeaters is the Duan–Lukin–Cirac–Zoller (DLCZ) scheme[3], whereby collective spin excitations in atomic ensembles[7] are used to provide the required quantum memory, and the heralded entanglement connection is used to boost the scaling of efficiency through memory enhancement. Many impressive experimental advances have been reported with this approach[8–15]. Entanglement generation between two quantum memories (repeater nodes) has been reported using atomic or spin ensembles[12–15], as well as single atomic ions or diamond defect spins[16–20]. Memory enhancement in efficiencies has been observed in heralded entanglement generation[12,21] by employing atomic or optical quantum memories. Memory-accelerated quantum key distribution has been demonstrated recently[22] by sending weak coherent pulses to a middle node for Bell state measurements (BSMs). There is also an alternative approach for the realization of quantum repeaters, with an all-photonic scheme in which the requirement for the quantum memory is replaced by the preparation of a large repeater graph state[23]. This approach has recently demonstrated noticeable experimental progress[24,25]. For the memory-based approach to quantum repeaters, a goal that remains outstanding is demonstrating a change in scaling of efficiencies enabled by quantum memories for the entanglement connection of two quantum repeater segments—the key ingredient for the quantum repeater protocol to achieve efficient scaling.

In this Article, we report an experimental realization of entanglement connection between two quantum repeater segments with a quantum-memory-enhanced scaling of its connection efficiencies. Compared with the direct entanglement swapping of two synchronous entangled photon pairs without the use of quantum memories[26], we demonstrate that the efficiency in the entanglement connection of two segments improves from a quadratic scaling to a linear scaling with the preparation efficiency of each entangled pair. This change in scaling of efficiencies, when extended to multiple segments, is key to the quantum repeater protocol improving from an exponential scaling to a polynomial scaling[2–4]. A challenging requirement for demonstrating the scaling change in the entanglement connection is that the coherence time of the quantum memories has to be longer than the preparation and successful heralding time of each entangled pair. In our experiment, with the help of optical traps, we have two atomic quantum memories with storage times of tens of milliseconds, long enough for on-demand entanglement swapping. Atom–photon entanglement is generated asynchronously in two long-lived quantum memories, and the entanglement swapping between them is implemented on demand only when both sides have successfully registered a photon (in general at different times). This experiment, as a demonstration of the change in scaling in the efficiencies for entanglement connection of two quantum repeater segments, provides a key enabling ingredient for the realization of larger-scale quantum repeaters and quantum networks.

Results

As illustrated in Fig. 1a, the key idea of the quantum repeater architecture is to divide the communication channel into multiple segments, establish entanglement for each segment, which is stored in quantum memories, and then to use entanglement swapping to connect these segments when each segment of entanglement has been heralded successfully. Here, we consider the demonstration

[1]Center for Quantum Information, IIIS, Tsinghua University, Beijing, China. [2]Present address: Institute for Experimental Physics, University of Innsbruck, Innsbruck, Austria. [3]Present address: Department of Physics, Beijing Normal University, Beijing, China. [4]These authors contributed equally. Yun-Fei Pu, Sheng Zhang. ✉e-mail: lmduan@tsinghua.edu.cn

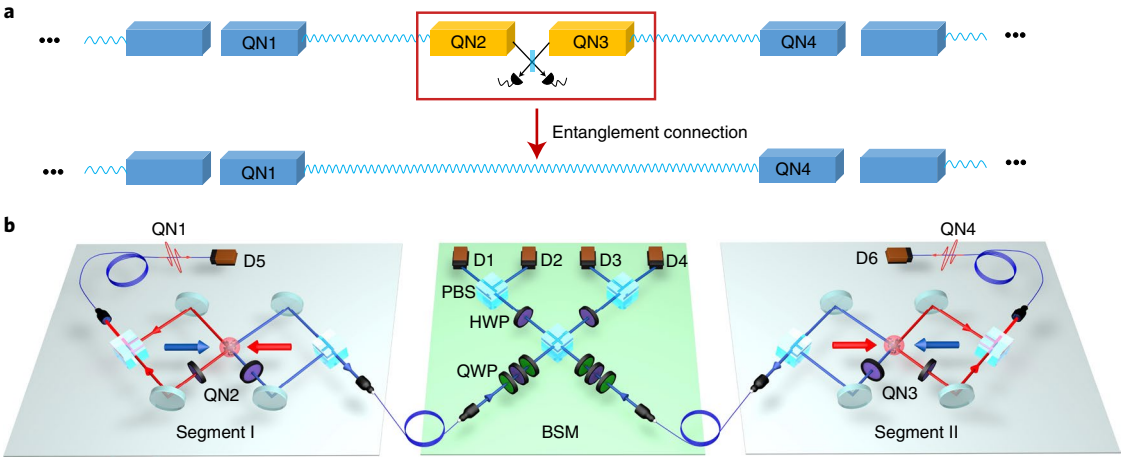

Fig. 1 | The quantum repeater protocol and the experimental set-up. a, A sketch of entanglement connection (swapping) in the quantum repeater protocol. QN represents a quantum repeater node. **b**, The whole experimental set-up consists of three parts: segment I (QN1 and QN2) and segment II (QN3 and QN4), together with a Bell state measurement (BSM) station in the centre. QN2 and QN3 are two similar atomic memory nodes separated by 3 m in space. QN1 and QN4 are photons in this experiment and are measured by detectors D5 and D6. A sandwich structure consisting of a quarter-wave plate (QWP), a half-wave plate (HWP) and another QWP is introduced to compensate for the polarization change in the fibre transmission. The coincidence events between the single-photon detectors D1 and D4 (or D2 and D3) project the two idler photons onto one of the four Bell states $|\Phi^+\rangle$.

of this architecture for the primitive case with two segments. As the two end nodes QN1 and QN4 do not need further connection, they can be measured according to the application protocol (such as for entanglement-based quantum key distribution[3,27]) before the connection of two middle nodes, QN2 and QN3. Therefore, in this simplified configuration, we do not need a quantum memory for the end nodes QN1 and QN4. In our experiment, we implement the qubits at QN1 and QN4 with photons and the qubits at QN2 and QN3 with atomic quantum memories, as shown in Fig. 1b. We generate atom–photon entanglement for each segment and perform on-demand entanglement swapping on the atomic memory qubits QN2 and QN3 through a Bell measurement, only when detectors D5 and D6 at nodes QN1 and QN4 have both successfully heralded registration of a photon count. Note that, unlike the configuration in ref. [14], which generates entanglement between two edge atomic memory nodes by simultaneous heralding of two photon counts in the middle, it is critical here that the middle nodes QN2 and QN3 are quantum memories so that we can store heralded states prepared asynchronously in these memories for an efficient entanglement connection.

In both QN2 and QN3, a coherence time of tens of milliseconds inside ^{87}Rb atomic ensembles is achieved through spatial confinement with an optical lattice[28–30]. A one-dimensional (1D) optical lattice holds the atoms and suppresses their motional decoherence by confining the atoms inside a single pancake potential of the lattice. Clock states ($|g\rangle \equiv |5S_{1/2}, F=2, m_F=0\rangle \leftrightarrow |s\rangle \equiv |5S_{1/2}, F=1, m_F=0\rangle$) are used to minimize the influence of the temporal and spatial fluctuation noise of the magnetic field[28], and a magic-value magnetic field of $B \approx 4.3$ G is employed to cancel the differential a.c. Stark shift induced by the lattice intensity inhomogeneity[29,30], as shown in Fig. 2a. The short-term ($\leq$1 ms) storage efficiency of QN2 is measured by the DLCZ scheme, as shown in Fig. 2b. The fast decay in this period is induced by the atomic motion inside a single lattice pancake[28,29]. The long-term (>1 ms) lifetime of the quantum memory in each node is measured by electromagnetically induced transparency (EIT) storage[30,31], as described in detail in the Supplementary Information. As illustrated in Fig. 2c, the long-term EIT storage time is 77 ± 3 ms and 14 ± 1 ms for QN2 and QN3, respectively. We attribute the large discrepancy between the lifetimes of the two memories to the imperfect geometry of the probe, the control and the lattice beams, which induces imperfect suppression of motional decoherence, as well as instability of the magnetic field due to power supply noise at QN3.

We use a variation of the DLCZ scheme to generate the atom–photon entanglement in each segment. The quantum information in the atomic ensemble is carried by the two magnetic-field-insensitive levels $|g\rangle$ and $|s\rangle$ in the ground-state manifold[3,28]. After the atoms are loaded into the 1D optical lattice and are optically pumped to the initial state $|g\rangle$, a weak write pulse in linear polarization drives a Raman transition from $|g\rangle$ to $|s\rangle$. We collect photons in two symmetric signal modes S_L and S_R with angles of $\pm 1.5°$ relative to the write beam, and two spatial modes of the spin–wave excitation, L and R, are defined correspondingly in the atomic cloud[14]. After we combine the two signal photon modes S_L and S_R on a polarizing beamsplitter (PBS2), as shown in Fig. 2a, and ignore the small higher-order excitation terms, the resulting atom–photon entangled state can be expressed as (with the vacuum part neglected as it will be eliminated by the subsequent measurements)

$$|\Psi\rangle_{S-A} = \frac{1}{\sqrt{2}}(|H\rangle|L\rangle + e^{i\phi_S}|V\rangle|R\rangle) \quad (1)$$

where $|H\rangle/|V\rangle$ represents the horizontal/vertical polarization of the signal photon, $|L\rangle/|R\rangle$ represents a single collective excitation in spatial mode L/R and ϕ_S is the phase difference between the two signal paths before they are combined on PBS2.

To evaluate the quality of the generated atom–photon entanglement in each segment, we coherently convert the spin–wave $|L\rangle$ and $|R\rangle$ into two idler photon modes I_L and I_R with a read pulse resonant to the transition $|s\rangle \rightarrow |e\rangle$ propagating in the opposite direction to the write beam. After the two idler modes are combined on PBS1 (Fig. 2a), the signal–idler photon state can be expressed as $|\Psi\rangle_{S-I} = \frac{1}{\sqrt{2}}(|H\rangle_S|H\rangle_I + e^{i(\phi_S+\phi_I)}|V\rangle_S|V\rangle_I)$, where ϕ_I is the propagation phase difference in paths I_L and I_R. To keep the total phase $\phi_S+\phi_I$ constant, we actively stabilize the path difference between L and R. Through quantum state tomography, the density matrix of this entangled state is reconstructed via the maximum likelihood method, and the fidelity with a two-qubit maximally entangled state is over 90% for both QN2 with a storage time varying from 10 μs to 1 ms and QN3 at 10 μs (Fig. 2b). We attribute the infidelity mainly to the imperfect optical pumping and the signal-to-noise ratio in the retrieval process of the idler photon.

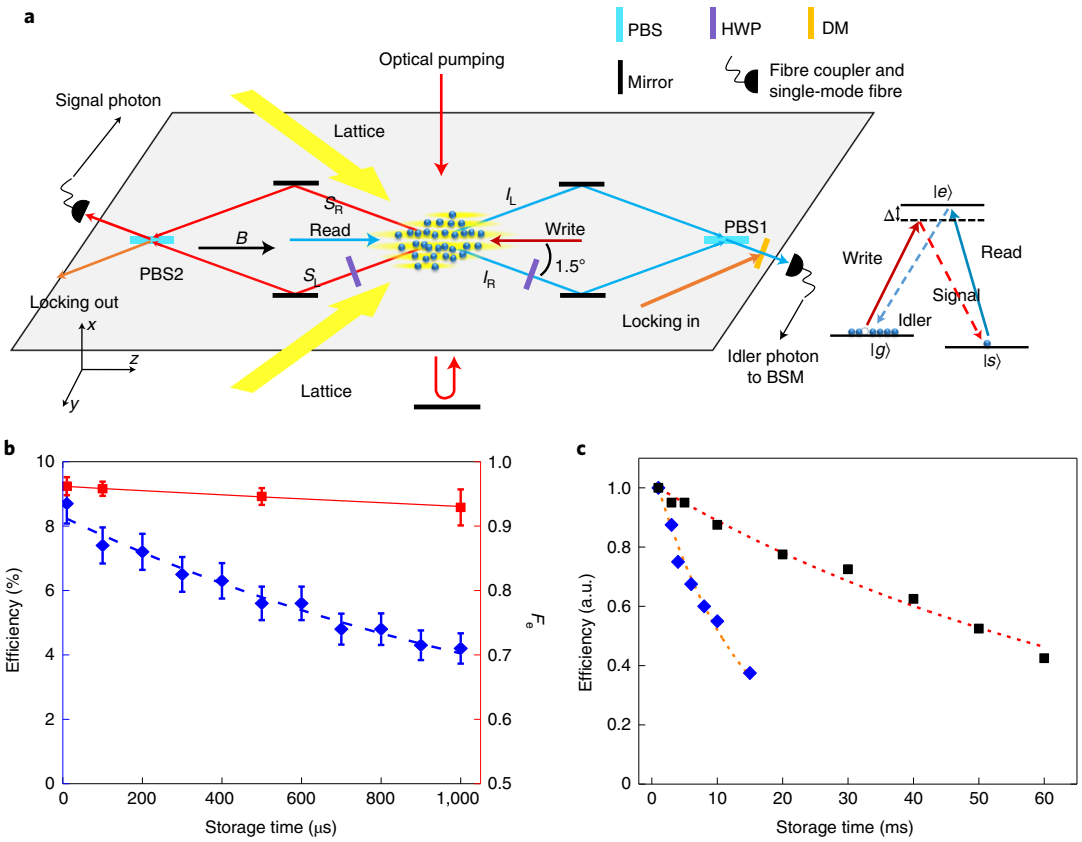

Fig. 2 | The quantum repeater node with long memory time. a, A zoom-in of QN1 (a signal photon) and QN2 (an atomic quantum memory). **b**, Short-term overall retrieval efficiency (blue diamonds) and the atom–photon entanglement fidelity F_e (red squares) within 1-ms storage in QN2. In both plots the error bars represent one standard deviation. **c**, Long-term storage efficiency measured by EIT storage at QN2 (black squares) and QN3 (blue diamonds), normalized to the time point of $t = 1$ ms. The plots are fitted with an exponential function (red and orange dashed lines). The $1/e$ lifetimes of QN2 and QN3 are 77 ± 3 ms and 14 ± 1 ms, respectively.

The protocol in this experiment can be split into three steps: the asynchronous preparation of atom–photon entanglement in segment I (QN1 and QN2) and segment II (QN3 and QN4), and the following entanglement connection, as shown in Fig. 3a. In step I, we generate atom–photon entanglement between QN1 and QN2 with a write–clean pulse train repeated at a rate of 1 MHz (Supplementary Information). Once a signal photon is recorded by the detector, the write–clean cycle halts and the sequence enters step II immediately.

In step II, we generate the atom–photon entanglement between QN3 and QN4 in a similar way as in step I. The difference, here, is that once the number of write–clean trials reaches 1,000, which is ~1 ms after generation of atom–photon entanglement in segment I, the whole sequence will terminate and restart from step I. This 1-ms window is determined as a trade-off between the near-deterministic detection of a signal photon at QN4 and the low decoherence of the established atom–photon entanglement in segment I during this window. As an example, with a medium overall signal photon detection probability of $p = 0.3\%$, which corresponds to an intrinsic excitation probability of $\chi \approx 1\%$, 1,000 trials yield a nearly deterministic success probability of $1-(1-0.3\%)^{1,000} \approx 95\%$ to generate the atom–photon entanglement. On the other hand, with the long coherence time of QN2, the atom–photon entanglement fidelity in segment I changes only slightly in the 1-ms window, and remains as high as $92.9 \pm 2.8\%$ at 1 ms, as illustrated in Fig. 2b. Although the retrieval efficiency decays to about one-half of the initial value within the first 1 ms, it only influences the entanglement swapping efficiency by a constant factor, which will not change the scaling. After the successful detection of a signal photon at QN4, the sequence proceeds to step III.

In many previous atom–photon entanglement experiments where two Zeeman sublevels are employed as the bases of stationary qubits[17,18,32,33], the phase in the established atom–photon entangled state oscillates due to the different Larmor precession rates of these two bases. For the asynchronous connection of two segments in a quantum repeater protocol, serious problems will appear due to the random entanglement preparation time between adjacent segments and hence the random accumulated phase. Here, in our experiment, the two bases of the stationary qubit $|L\rangle$ and $|R\rangle$ are nearly identical, except the spatial orientation of the spin–wave vectors, which have no influence on the phase[14]. Accordingly, our established atom–photon entanglement (equation (1)) in each node has a time-independent phase ϕ_S (Supplementary Information), which guarantees that the final entangled state after entanglement connection will have a constant phase no matter when the entanglements are prepared in the two segments.

After the successful detection of two signal photons in steps I and II, we connect the two segments through entanglement swapping and entangle QN1 and QN4 (two signal photons) in a post-selected way in step III. We coherently convert the spin–wave qubits in the two memories to idler photons, which are further directed to the middle station to perform the joint BSM in the photonic polarization basis (Fig. 1b). After the successful entanglement swapping between QN2 and QN3, the two signal photons are projected into a maximally entangled state

$$|\Psi\rangle_{S-S} = \frac{1}{\sqrt{2}}(|H\rangle_1|H\rangle_4 + e^{i(\phi_I+\phi_{II})}|V\rangle_1|V\rangle_4) \quad (2)$$

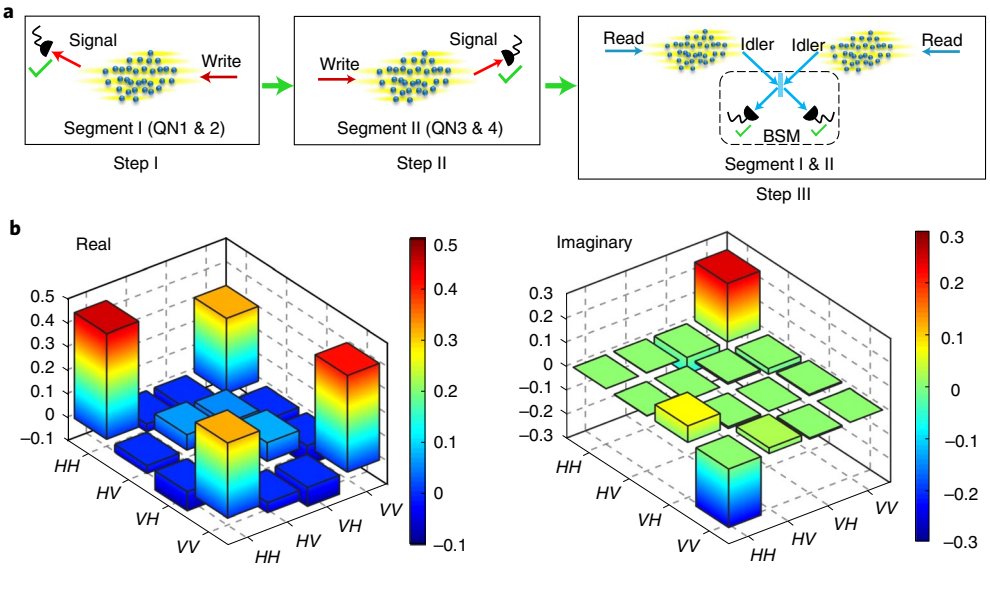

c

Entanglement fidelity					
Step I				Step II	Step III
I (10 μs)	I (100 μs)	I (500 μs)	I (1,000 μs)	II (10 μs)	Signal–signal
96.2 ± 1.4%	95.8 ± 1.1%	94.6 ± 1.3%	92.9 ± 2.8%	90.6 ± 1.6%	79.5 ± 4.8%

Fig. 3 | Entanglement connection of two quantum repeater segments. a, The protocol of the asynchronous generation and connection of entanglement. **b**, The reconstructed density matrix of the signal–signal state after entanglement swapping. The fidelity of the reconstructed state to the nearest maximally entangled state is 79.5 ± 4.8%. The density matrix shown here represents the average over all the entangled states from 1,000 trials. Although the quality of the final entanglement depends on how long the heralded state is stored in QN2, this dependence is weak as the coherence loss in QN2 is small in this experiment. The whole data acquisition time is 16 h for all the 16 measurement bases of the final QN1–QN4 state, and the total number for the recorded four-photon coincidence count is 656. **c**, The atom–photon entanglement fidelity in segment I after storage times of 10 μs, 100 μs, 500 μs and 1,000 μs, and in segment II after a storage of 10 μs, together with the final signal–signal entanglement fidelity. Error bars represent one standard deviation.

where $H(V)_{1(4)}$ represents a signal photon in the horizontal (vertical) polarization basis at QN1(4), and $\phi_{\mathrm{I}}+\phi_{\mathrm{II}}$ is a constant phase including all the path phases in the write and read processes in both segments. We perform quantum state tomography on this signal photon entangled state by setting proper polarization measurement bases before detectors D5 and D6, and reconstruct the density matrix with the maximum likelihood method (Fig. 3b). With the atom–photon entanglement generation probabilities in both segments I and II set to 0.1%, the fidelity of the reconstructed signal–signal entangled state to a maximally entangled state is measured to be 79.5 ± 4.8%, which is clear evidence of the generated entanglement between QN1 and QN4 and confirms the success of the whole protocol.

Finally, we investigate the scaling property of our protocol. Suppose the success probability of generating atom–photon entanglement on both sides is set to p. If $p > 1/n$, where n is the maximally allowed trial number in the write process of segment II, the atom–photon entanglement in segment II can be prepared nearly deterministically. The expected number of trials to successfully generate the entanglement on both sides and to perform a successful entanglement swapping is thus proportional to $2C/p$, which is linearly dependent on $2/p$, with a varying coefficient $C(p,n) \in (1,1.42)$ (Supplementary Information). By comparison, without the memory enhancement, the successful entanglement connection will require simultaneous entanglement generation on both sides and therefore the number of trials scales as $1/p^2$. Here, we verify that the overall success rate of entanglement generation and connection between the two segments is linearly dependent on p (that is, the expected time or trial number is $O(1/p)$, where $O(1/p)$ denotes the order of $1/p$) by measuring the four-photon coincidence rate with the two signal photons in $|H\rangle_1$ and $|H\rangle_4$ and the two idler photons detected in the BSM, which is one-half of the signal–signal entanglement generation rate in our case (equation (2)). As shown in Fig. 4, when p is varied, the signal–signal entanglement is generated at a rate linearly dependent on the excitation probability p in each segment, which confirms the fundamental acceleration in entanglement connection from a quadratic scaling to a linear scaling for the two-segment case. In Fig. 4, we also compare the four-photon coincidence rates between this memory-enhanced protocol and a corresponding entanglement swapping protocol without use of the quantum memories (Supplementary Information), and we can see that the advantage of the memory-enhanced protocol is more evident at a smaller p due to the improved scaling with $O(p)$.

Discussion

In summary, we have demonstrated the entanglement connection of two quantum repeater segments with improved scaling in efficiencies through enhancement by quantum memories. In the future, this set-up may be combined with a frequency conversion set-up to convert the photons on each side to the telecom wavelength so that the communication length of each segment can be extended to tens of kilometres[15,34,35]. The scaling change from a quadratic dependence on the generation rate of each segment to a linear dependence can then be used to remarkably boost the overall communication efficiency, which is a key advantage of the quantum repeater protocol compared with the direct communication scheme. This work thus demonstrates an important primitive of the quantum repeater protocol and provides a building block for the implementation of

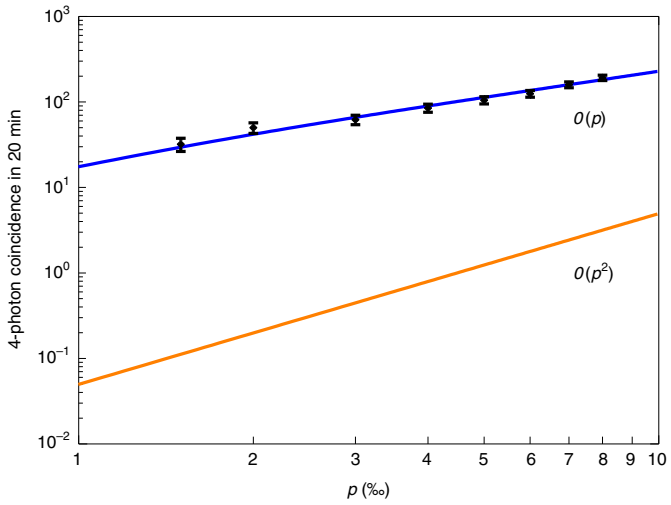

Fig. 4 | Memory-enhanced scaling of efficiencies for entanglement connection. Four-photon coincidence counts in 20 min are measured at an excitation probability of p varying from 0.15% to 0.8% (black diamonds). Error bars represent one standard deviation. The blue solid curve is the theoretical four-photon coincidence rate in our experiment and the orange curve is the calculated four-photon rate of the same entanglement swapping protocol but without use of the quantum memories (Supplementary Information). For these two cases (with or without use of the quantum memories), the fidelity of the final state should be comparable, as the additional fidelity decay induced by the coherence loss in the quantum memory, which is ~3% for the required maximal 1-ms storage time from Fig. 3c, is much less than the overall infidelity of the final state, measured to be around 20% and mainly from the contribution of the technical noise in entanglement swapping and the addition of the infidelities from the two-segment Einstein–Podolsky–Rosen (EPR) states. However, the efficiency improves from a quadratic dependence ($O(p^2)$) to a linear scaling ($O(p)$) by use of the memory enhancement.

long-distance quantum communication and large-scale quantum networks.

Online content

Any methods, additional references, Nature Research reporting summaries, source data, extended data, supplementary information, acknowledgements, peer review information; details of author contributions and competing interests; and statements of data and code availability are available at https://doi.org/10.1038/s41566-021-00764-4.

Received: 29 September 2020; Accepted: 17 January 2021;
Published online: 25 February 2021

References

1. Kimble, H. J. The quantum internet. *Nature* **453**, 1023–1030 (2008).
2. Briegel, H.-J., Dür, W., Cirac, J. I. & Zoller, P. Quantum repeaters: the role of imperfect local operations in quantum communication. *Phys. Rev. Lett.* **81**, 5932–5935 (1998).
3. Duan, L.-M., Lukin, M. D., Cirac, J. I. & Zoller, P. Long-distance quantum communication with atomic ensembles and linear optics. *Nature* **414**, 413–418 (2001).
4. Sangouard, N., Simon, C., de Riedmatten, H. & Gisin, N. Quantum repeaters based on atomic ensembles and linear optics. *Rev. Mod. Phys.* **83**, 33–80 (2011).
5. Bennett, C. H. et al. Teleporting an unknown quantum state via dual classical and Einstein–Podolsky–Rosen channels. *Phys. Rev. Lett.* **70**, 1895–1899 (1993).
6. Bennett, C. H. et al. Purification of noisy entanglement and faithful teleportation via noisy channels. *Phys. Rev. Lett.* **76**, 722–725 (1996).
7. Hammerer, K., Sorensen, A. S. & Polzik, E. S. Quantum interface between light and atomic ensembles. *Rev. Mod. Phys.* **82**, 1041–1093 (2010).
8. Chou, C.-W. et al. Measurement-induced entanglement for excitation stored in remote atomic ensembles. *Nature* **438**, 828–832 (2005).
9. Chaneliere, T. et al. Storage and retrieval of single photons transmitted between remote quantum memories. *Nature* **438**, 833–836 (2005).
10. Eisaman, M. D. et al. Electromagnetically induced transparency with tunable single-photon pulses. *Nature* **438**, 837–841 (2005).
11. Simon, J., Tanji, H., Ghosh, S. & Vuletic, V. Single-photon bus connecting spin–wave quantum memories. *Nat. Phys.* **3**, 765–769 (2007).
12. Chou, C.-W. et al. Functional quantum nodes for entanglement distribution over scalable quantum networks. *Science* **316**, 1316–1320 (2007).
13. de Riedmatten, H., Afzelius, M., Staudt, M. U., Simon, C. & Gisin, N. A solid-state light–matter interface at the single-photon level. *Nature* **456**, 773–777 (2008).
14. Yuan, Z.-S. et al. Experimental demonstration of a BDCZ quantum repeater node. *Nature* **454**, 1098–1101 (2008).
15. Yu, Y. et al. Entanglement of two quantum memories via fibres over dozens of kilometres. *Nature* **578**, 240–245 (2020).
16. Bernien, H. et al. Heralded entanglement between solid-state qubits separated by three metres. *Nature* **497**, 86–90 (2013).
17. Moehring, D. L. et al. Entanglement of single-atom quantum bits at a distance. *Nature* **449**, 68–71 (2007).
18. Stephenson, L. J. et al. High-rate, high-fidelity entanglement of qubits across an elementary quantum network. *Phys. Rev. Lett.* **124**, 110501 (2020).
19. Slodička, L. et al. Atom–atom entanglement by single-photon detection. *Phys. Rev. Lett.* **110**, 083603 (2013).
20. Hofmann, J. et al. Heralded entanglement between widely separated atoms. *Science* **337**, 72–75 (2012).
21. Kaneda, F., Xu, F., Chapman, J. & Kwiat, P. G. Quantum-memory-assisted multi-photon generation for efficient quantum information processing. *Optica* **4**, 1034–1037 (2017).
22. Bhaskar, M. K. et al. Experimental demonstration of memory-enhanced quantum communication. *Nature* **580**, 60–64 (2020).
23. Azuma, K., Tamaki, K. & Lo, H.-K. All-photonic quantum repeaters. *Nat. Commun.* **6**, 6787 (2015).
24. Li, Z.-D. et al. Experimental quantum repeater without quantum memory. *Nat. Photon.* **13**, 644–648 (2019).
25. Hasegawa, Y. et al. Experimental time-reversed adaptive Bell measurement towards all-photonic quantum repeaters. *Nat. Commun.* **10**, 378 (2019).
26. Zhao, Z. et al. Experimental realization of entanglement concentration and a quantum repeater. *Phys. Rev. Lett.* **90**, 207901 (2003).
27. Ekert, A. K. Quantum cryptography based on Bell's theorem. *Phys. Rev. Lett.* **67**, 661–663 (1991).
28. Zhao, R. et al. Long-lived quantum memory. *Nat. Phys.* **5**, 100–104 (2009).
29. Yang, S.-J., Wang, X.-J., Bao, X.-H. & Pan, J.-W. An efficient quantum light–matter interface with sub-second lifetime. *Nat. Photon.* **10**, 381–384 (2016).
30. Dudin, Y. O., Zhao, R., Kennedy, T. A. B. & Kuzmich, A. Light storage in a magnetically dressed optical lattice. *Phys. Rev. A* **81**, 041805 (2010).
31. Fleischhauer, M. & Lukin, M. D. Dark-state polaritons in electromagnetically induced transparency. *Phys. Rev. Lett.* **84**, 5094–5097 (2000).
32. Stute, A. et al. Tunable ion–photon entanglement in an optical cavity. *Nature* **485**, 482–485 (2012).
33. Yang, S.-J. et al. Highly retrievable spin–wave–photon entanglement source. *Phys. Rev. Lett.* **114**, 210501 (2015).
34. Krutyanskiy, V. et al. Light–matter entanglement over 50 km of optical fibre. *npj Quantum Inf.* **5**, 72 (2019).
35. Chang, W. et al. Long-distance entanglement between a multiplexed quantum memory and a telecom photon. *Phys. Rev. X* **9**, 041033 (2019).

Methods
Methods are included in the Supplementary Information.

Data availability
The data that support the plots within this paper and other findings of this study are available from the corresponding author upon reasonable request.

Code availability
The code used for quantum state tomography is available from the corresponding author upon reasonable request.

Acknowledgements
This work was supported by the National Key Research and Development Program of China (2016YFA0301902), the Beijing Academy of Quantum Information Sciences, the Frontier Science Center for Quantum Information of the Ministry of Education of China and the Tsinghua University Initiative Scientific Research Program. Y.K.W. acknowledges support from the Shuimu Tsinghua Scholar Program and the International Postdoctoral Exchange Fellowship Program.

Author contributions
L.-M.D. designed the experiment and supervised the project. Y.-F.P., S.Z., N.J., W.C. and C.L. performed the experiment. Y.-F.P. and S.Z. analysed the data. Y.-K.W. contributed materials and analysis tools. Y.-F.P., S.Z., Y.-K.W. and L.-M.D. wrote the manuscript.

Competing interests
The authors declare no competing interests.

Additional information
Supplementary information The online version contains supplementary material available at https://doi.org/10.1038/s41566-021-00764-4.

Correspondence and requests for materials should be addressed to L.-M.D.

Peer review information *Nature Photonics* thanks Bing Qi and the other, anonymous, reviewer(s) for their contribution to the peer review of this work.

Reprints and permissions information is available at www.nature.com/reprints.